Journal of Science and Technology in Civil Engineering, HUCE, 2024, 18 (4): 30–40

EFFECT OF NANO-CALCIUM CARBONATE ON MECHANICAL PROPERTIES OF INTERFACIAL TRANSITION ZONE BETWEEN FIBER SURFACE AND CONCRETE

Dang Van Phi[a,*], Ngo Tri Thuong[b]

[a]*Department of Civil Engineering, Hanoi University of Mining and Geology, 18 Vien street, Bac Tu Liem district, Hanoi, Vietnam*
[b]*Department of Civil Engineering, Thuyloi University, 175 Tay Son street, Dong Da district, Hanoi, Vietnam*

Article history:
Received 01/11/2024, Revised 16/12/2024, Accepted 20/12/2024

Abstract

This study investigated the effect of nano-$CaCO_3$ content on the hardness (H) and Young's modulus (E) at the interfacial transition zone (ITZ) surrounding fibers and ultra-high performance concrete (UHPC). Nano-$CaCO_3$ was incorporated at varying contents from 1% to 4% by weight of cement. The nanoindentation (NI) test and scanning electron microscopy (SEM) to examine the mechanical properties and microstructures at the ITZ. The results of the study indicated that UHPC incorporating nano-$CaCO_3$ exhibited an improvement in both H and E at the ITZ compared to UHPC without nano-$CaCO_3$. Specifically, the H and E values for UHPC containing 3% nano-$CaCO_3$ were measured at 3.49 ± 0.15 and 51.47 ± 1.23 GPa, respectively, whereas those values of UHPC without any nano-$CaCO_3$ were 3.10 ± 0.12 and 49.44 ± 1.22 GPa, respectively. This enhancement in H and E at the ITZ is attributed to the toughening effects at the interface caused by the nano-$CaCO_3$, along with improved hydration. Besides, SEM images revealed that UHPC containing nano-$CaCO_3$ displayed a denser and more homogeneous microstructure compared to its counterpart without nano-$CaCO_3$. Furthermore, the addition of nano-$CaCO_3$ increased the compressive strength of UHPC by 1.47% to 9.49% as the content rose from 1% to 4%, attributed to improved particle packing and a more compact microstructure. In contrast, UHPC flowability declined as nano-$CaCO_3$ content increased, as indicated by a reduction in slump flow from 185 ± 15 mm to 160 ± 5 mm, which is associated with increased water absorption by the extensive surface area of the material.

Keywords: Nano-$CaCO_3$, hardness, Young's modulus, interfacial transition zone, UHPC.

https://doi.org/10.31814/stce.huce2024-18(4)-03

1. Introduction

Ultra-high-performance concrete is characterized by a high binder content, which significantly enhances its mechanical properties and durability. UHPC is formulated with a low water-to-binder ratio, promoting a denser mixture that contributes to its strength [1]. UHPC are extremely heterogeneous materials because of their various constituent phases and diverse processing conditions. The microstructure and overall properties of UHPC are influenced by the source materials, mixture ratios, curing conditions, and hydration rate [1, 2]. Although UHPC exhibits significantly lower porosity compared to conventional concrete, it still contains a relatively weak ITZ of mixtures [3]. This zone exists at the interface between cement paste and aggregate or fiber, which significantly influences the overall strength and durability of concrete. Thus, enhancing the mechanical properties of the ITZ is crucial for improving the long-term performance of UHPC. However, the characteristics and thickness of ITZs depend on the type of fiber, hydration level, and water-to-cement ratio [4, 5, 6].

*Corresponding author. *E-mail address:* dangvanphi@humg.edu.vn (Phi, D. V.)

The use of materials with fine particle sizes in the composition is expected to improve the microstructure of ITZ and the overall strength of concrete [3]. This process involves incorporating a significant amount of supplementary cementitious materials, such as silica fume, slag, and fly ash, along with a smaller quantity of nano-materials [7, 8, 9, 10]. These materials contribute to filling voids within the mixture, improving the interlocking of particles, and ultimately leading to a more robust and durable concrete formulation [7, 8]. Wu et al. [9] reported that the optimal silica fume content in UHPC is 15% to 25%, leading to a 170% increase in bond strength at 28 days compared to samples without silica fume. The addition of nanomaterials (NMs), such as nano-CNTs, nano-TiO_2, and nano-Al_2O_3, has enhanced the mechanical strength of concrete, primarily due to their extremely small particle size and superior pozzolanic reactivity [11, 12]. Zhang et al. [11] investigated the influence of nano-CNTs on the flexural strength of concrete. Their findings demonstrated that substituting 0.05% of cement with nano-CNTs resulted in an increase in the flexural strength of concrete up to 68%. Su et al. [12] replaced 3.0% of cement with different NMs in UHPC composition. Their results indicated that compressive strength significantly improved depending on the type and amount of NMs used. Besides, nano-TiO_2 produced the highest compressive strength at 162.6 MPa, while nano-Al_2O_3 resulted in the lowest at 143.5 MPa.

In recent years, the use of nano-$CaCO_3$ in concrete has become more common because nano-$CaCO_3$ can significantly improve the compressive and flexural strength of UHPC due to its high surface area and reactivity, leading to a more refined microstructure [13]. Several studies have indicated that the physical properties of $CaCO_3$ may offer benefits for the development of cementitious systems [14, 15, 16]. The presence of $CaCO_3$ nanoparticles creates a seeding effect, promoting the rapid formation of calcium silicate hydrate (C-S-H) through their interaction with the surfaces of C_3S particles [17]. Shaikh and Supit [14] investigated the influence of nano-$CaCO_3$ on the compressive strength and durability of high-volume fly ash concretes, which contain 40% and 60% fly ash. Their results indicated that the early-age compressive strength of concrete with 1% nano-$CaCO_3$ is approximately 146–148% higher than that of conventional concrete. Xu et al. [15] indicated that the addition of 0.5% nano-$CaCO_3$ reduced the effectiveness of calcium nitrite as an early strength agent, whereas dosages of 1% and 2% increased concrete strength by 13% and 18% at standard curing temperatures and 17% and 14% at low curing temperatures after 3 days. Wu et al. [16] reported that the mechanical strength of UHPC improved as the nano-$CaCO_3$ content increased, reaching a maximum of 3.2%. At this dosage, the 28-day bond strength, compressive strength, and flexural strength increased by around 40%, 10%, and 20%, respectively, compared to the control mixture.

Although the effects of NMs on key mechanical properties of concrete, including bond strength, compressive strength, and flexural strength, have been explored in aforementioned studies, however, there remains a significant gap in the literature concerning the microstructural properties at ITZ of reinforced concrete enhanced with NMs. Thus, the study aimed to analyze the effects of nano-$CaCO_3$ on the mechanical properties of the ITZ that exists between steel fiber surfaces and UHPC. The inclusion of nano-$CaCO_3$ in UHPC is predicted to improve the strength of the ITZ of UHPC through their filling properties, combined with their chemical interactions. The primary objectives of this study were to assess the influence of nano-$CaCO_3$ content on the hardness and modulus of the ITZ, as well as the mechanical properties of UHPC. These findings will provide important information useful for developing UHPC with superior performance.

2. Experiment

2.1. Materials and Sample Setup

Table 1 describes the compositions of the mixtures used in this study. The average particle diameters of cement, silica fume (98.5% SiO_2), and silica powder were 9.0 μm, 23.0 μm, and 5.0 μm, respectively. Nano-$CaCO_3$ composed of 98.0% $CaCO_3$, had an average particle size of 50 nm. Silica sand with an average grain size of 250 μm was utilized. Silica powder, which served as the filler in the matrices, contained 98.0% SiO_2 and exhibited a density of 2.6 g/m^3. To improve the workability of the matrices, polycarboxylate ether superplasticizers with 30% solid content were employed. Five different mixtures were prepared: UHPC without any nano-$CaCO_3$ (UHPC-0), UHPC containing 1% nano-$CaCO_3$ (UHPC-1), 2% nano-$CaCO_3$ (UHPC-2), 3% nano-$CaCO_3$ (UHPC-3), and 4% nano-$CaCO_3$ (UHPC-4). The quantities of nano-$CaCO_3$ are calculated according to the weight of the cement in the concrete formulation. The proportions of the mixture were determined based on the procedure outlined in reference [18], with modifications to the water and superplasticizer levels in this study to meet the requirements of the casting process when applied to nano-$CaCO_3$.

Table 1. The weight components for a mixture of $1.0 \times 1.0 \times 1.0$ m^3 (unit: kg)

Mixture	Cement	Nano-$CaCO_3$	Silica sand	Silica fume	Silica powder	Superplasticizer	Water
UHPC-0	836.18	0.00	919.80	209.04	250.85	58.53	175.60
UHPC-1	833.33	8.33	916.67	208.33	250.00	58.33	175.00
UHPC-2	830.51	16.61	913.56	207.63	249.15	58.14	174.41
UHPC-3	827.70	24.83	910.47	206.93	248.31	57.94	173.82
UHPC-4	824.92	33.00	907.41	206.23	247.47	57.74	173.23

This study utilized Ordinary Portland Cement, meeting the specifications of ASTM C150 Type 1 for hydraulic cement. The dry ingredients were blended for around 5 minutes. Afterward, water was gradually incorporated over 1 minute, with the mixture being continuously stirred for another 5 minutes. The superplasticizer was added gradually and mixed in for an additional 5 minutes. Further details on the mixing procedure are provided in the preceding study [19].

The NI samples were prepared following the steps, as outlined by Dang et al. [3]. The sample was cylindrical in shape, with precise dimensions of 31 mm in diameter and 10 mm in height. Moreover, the NI experimental design of this study included the application of steel fibers having a diameter of 0.3 mm and a length of 30 mm, along with an elastic modulus of 200 GPa. Each of the specimens utilized in the experiments was reinforced with nine steel fibers, thereby enabling a detailed analysis of their influence on the mechanical properties at the ITZ of mixtures.

2.2. Experimental setup and Testing procedure

Fig. 1 illustrates the equipment used to evaluate the workability of the mixtures. The apparatus resembles a truncated cone, featuring a height of 60 mm, a large base diameter of 100 mm, and a small base diameter of 70 mm. The procedure for assessing concrete workability adheres to the ASTM C1437 standard [20]. The cube samples of $50 \times 50 \times 50$ mm^3 were tested in accordance with ASTM C109/C109M-23 for compressive strength evaluation [21]. Fig. 2 shows the universal testing machine (UTM) employed for conducting compressive tests. During the experimental procedures, the load was continuously set at a speed of 1 mm/min. Testing for all specimens was conducted after a 28-day period in dry conditions.

The mechanical properties of the ITZ of mixtures were investigated by using the NHT2 Nanoindentation Tester by CSM Instruments, as shown in Fig. 3. A standard nanoindentation load-displacement

Figure 1. Mini slump flow equipment [22]

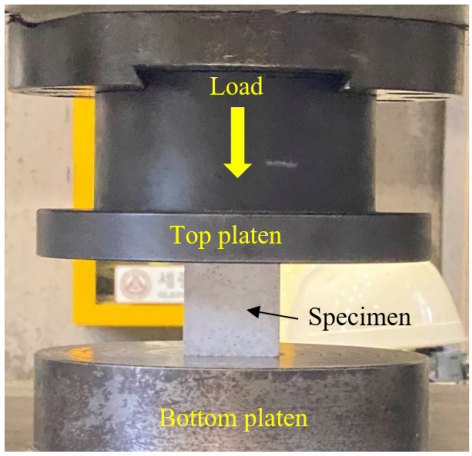

Figure 2. UTM used for compressive test

curve along with its relevant parameters is shown in Fig. 4. The maximum load applied during the NI tests was 2.0 mN, with the loading speed set at 1.0 mN/s. In this study, NI tests were conducted within the fiber mixture zone surrounding a steel fiber. Each mixture comprised 200 indented points which were discovered. Furthermore, Scanning Electron Microscopy was conducted to investigate the surface characteristics and microstructures present at the ITZ of the mixtures.

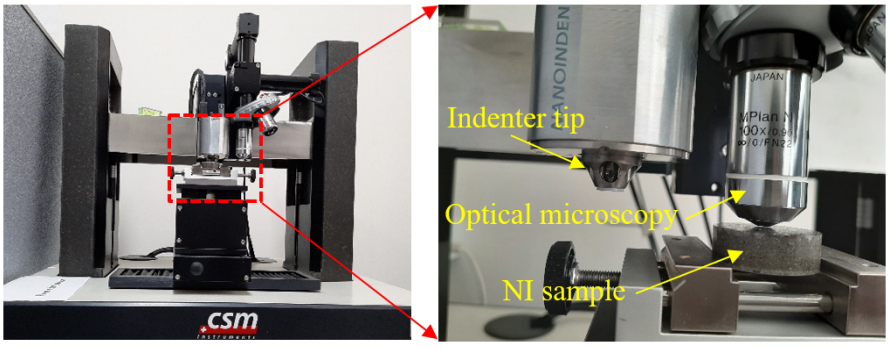

Figure 3. Nanoindentation testing systems

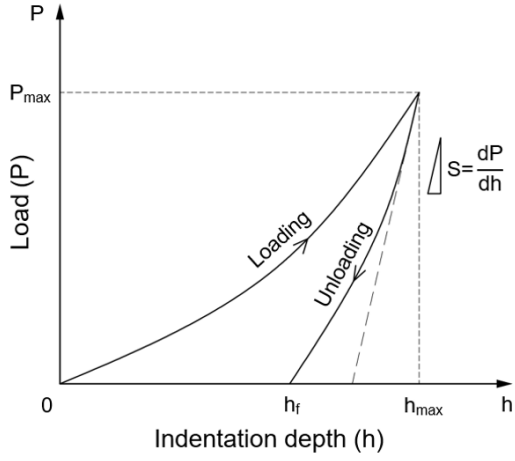

Figure 4. Typical load–depth curve in a nanoindentation test [23, 24]

The H and E are calculated by using the Oliver-Pharr method [25], as provided in Eqs. (1) and (2) [25, 26].

$$H = \frac{P_{\max}}{A_c} \tag{1}$$

$$E = \left(1 - \upsilon^2\right)\left(\frac{1}{E_r} - \frac{1 - \upsilon_i^2}{E_i}\right)^{-1} \tag{2}$$

where $P_{\max}$ is the peak load, A_c denotes the contact area, and υ is the Poisson's ratio of the samples. ν_i and E_i are Poisson's ratio and Young's modulus of the diamond indenter tip. The reduced modulus is indicated by E_r.

3. Results and Discussion

3.1. Influence of nano-$CaCO_3$ on mixture flowability

Fig. 5 presents typical images related to the mini-slump flow tests carried out on the mixtures, while the influence of nano-$CaCO_3$ levels on the flowability of mixtures is shown in Fig. 6. It is evident that the slump flow progressively decreased as the nano-$CaCO_3$ levels increased. As the

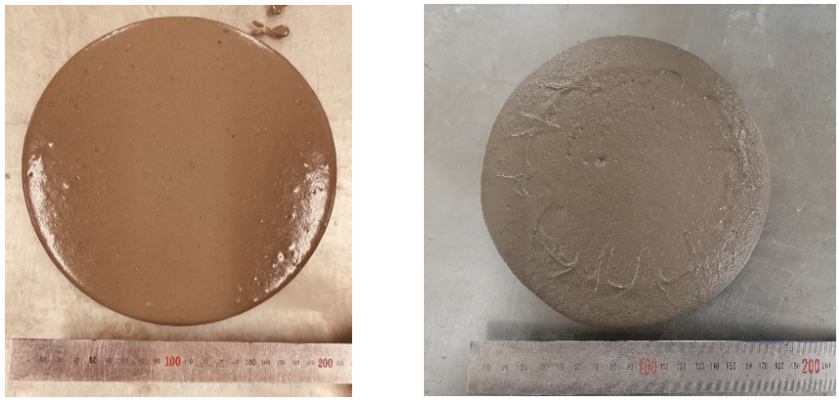

(a) UHPC-0 (b) UHPC-4

Figure 5. Typical flowability of the mixtures

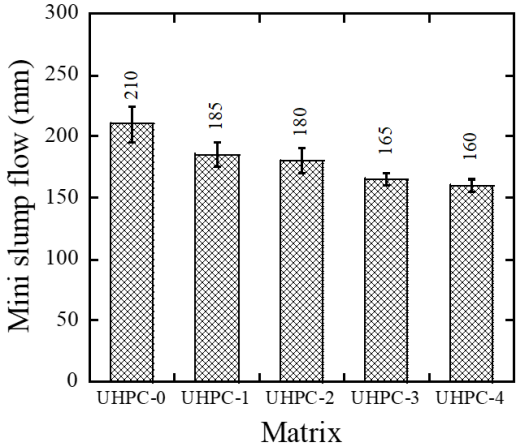

Figure 6. Mini slump flow of mixtures

contents of nano-$CaCO_3$ were increased from 1% to 4%, the flowability of UHPC decreased from 185 ± 15 to 160 ± 5 mm. This indicated that the addition of nanomaterials had a significant effect on the required water demand of mixtures. This demonstrates that the adding nano-$CaCO_3$ significantly affected the water requirements of the mixtures. The result is consistent with the findings observed in the research by Liu et al. [27]. Their results indicated that an increase in nano-$CaCO_3$ content led to a decline in flowability and a shorter setting time for the fresh cement paste. Although nano-$CaCO_3$ can occupy voids between the particles in mixtures, replacing some entrapped water, it ultimately results in an increase in the volume of free water [28].

3.2. Effects of nano-$CaCO_3$ contents on the compressive strength of mixtures

The incorporation of nano-$CaCO_3$ significant influence on the compressive strength of UHPC, as shown in Fig. 7. As the nano-$CaCO_3$ content varied between 1% and 4%, the compressive strength of UHPC increased by 1.47% to 9.49%, which was higher than the compressive strength of the control sample (UHPC-0). The compressive strength of UHPC containing 1%, 2%, 3%, and 4% nano-$CaCO_3$ was 192.18 ± 3.17, 194.33 ± 3.85, 202.51 ± 4.21, and 187.68 ± 2.98 MPa, respectively. All mixtures containing nano-$CaCO_3$ exhibited a higher compressive strength in comparison with UHPC-0 (184,96 ± 2.84 MPa), which did not contain any nano-$CaCO_3$. The enhanced strength of UHPC is attributed to the unique characteristics of nano-$CaCO_3$, which can improve particle packing and contribute to a denser microstructure, ultimately leading to improved strength performance. Dang et al. [23] reported that the nano-$CaCO_3$ improved the microstructure and enhanced the percentage of C-S-H of cement hydration products of mixtures based on the nuclear effects of nano-$CaCO_3$. However, as the amount of nano-$CaCO_3$ increased by over 3% incorporated in UHPC, the mechanical properties of UHPC decreased owing to the agglomeration of NMs [29, 30, 31]. The use of an excessive quantity of nano-$CaCO_3$ led to its agglomeration due to the fine particle size and extensive surface area of nano-$CaCO_3$. This phenomenon increased the viscosity and reduced the flowability of mixtures, resulting in more cracks and air voids in both the ITZ and the concrete microstructure.

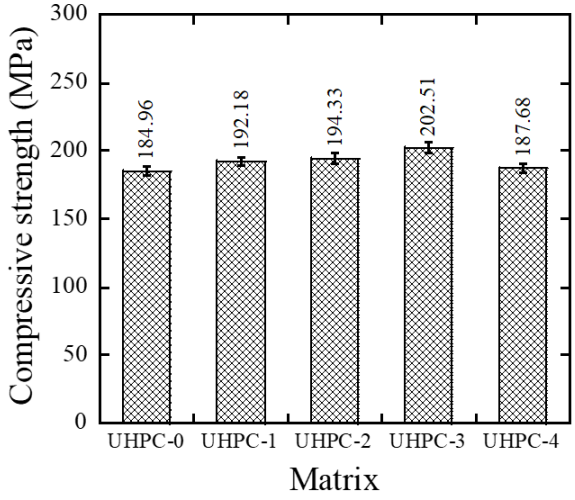

Figure 7. Compressive strength of mixtures

Fig. 8 illustrates the mixture samples following the completion of the compressive tests. The fractures present in the mixtures are incorporated into the overall failure and crack patterns observed. These patterns provide insight into the structural integrity and behavior of the materials under compressive stress. Explosive cracks are recognized in the samples of UHPC-0, UHPC-1, UHPC-2, and

UHPC-4, each exhibiting varying degrees of damage. In particular, UHPC formulations with nano-$CaCO_3$ displayed less damage while exhibiting a greater number of cracks. Especially, UHPC-3 did not reveal severe damage, however, it displays a considerable number of micro-cracks, as shown in Fig. 8.

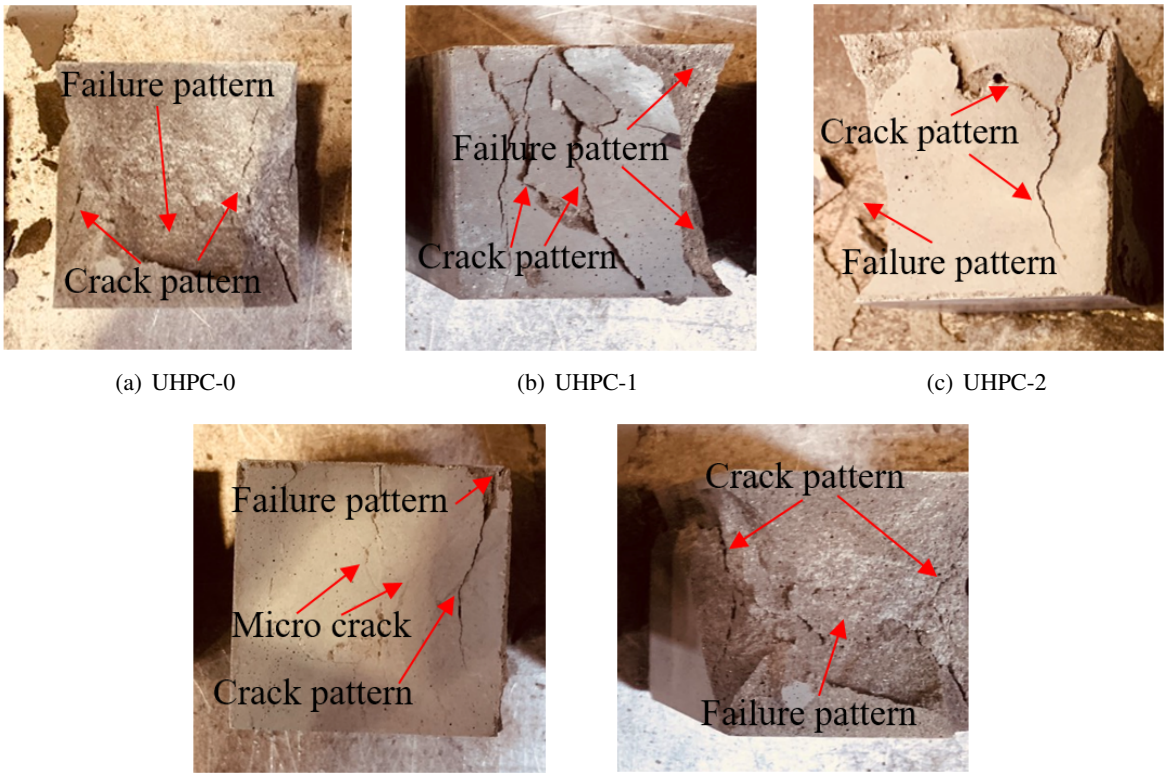

(a) UHPC-0 (b) UHPC-1 (c) UHPC-2

(d) UHPC-3 (e) UHPC-4

Figure 8. Failure and crack pattern occurring under compressive tests

3.3. Effects of nano-$CaCO_3$ contents on the mechanical properties of ITZs

Fig. 9 illustrates a typical surface morphology of the specimen within ITZ based on the results of the NI experiment. Following the completion of the unloading process, the surface exhibits indentations characterized by a triangular prism shape, which are attributable to the penetration of the indenter tip. The data on loads and displacement depths obtained from the NI tests were subsequently used to determine the mechanical properties (H and E) of ITZs, as described in Eqs. (1) and (2). Fig. 10 presents the H and E at ITZ of UHPC-0, UHPC-1, UHPC-2, UHPC-3 and UHPC-4. The UHPC-3 demonstrated the highest H and E values, which were 3.49 ± 0.15 and 51.47 ± 1.23 GPa, respectively, whereas UHPC-0 produced the lowest ones of 3.10 ± 0.12 and 49.44 ± 1.22

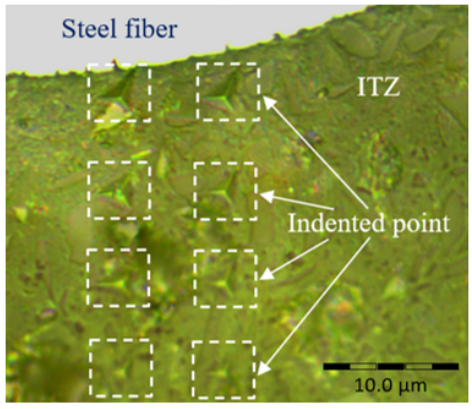

Figure 9. Indented points surrounding fiber and mixture

GPa, respectively. The significant enhancement in both H and E is primarily explained by the action of nanoparticles, which may have induced interfacial toughening as a result of their compact structure and/or enhanced hydration products [28]. Besides, the nucleation effect of nano-$CaCO_3$ can improve the microstructure and elevate the levels of C–S–H [23].

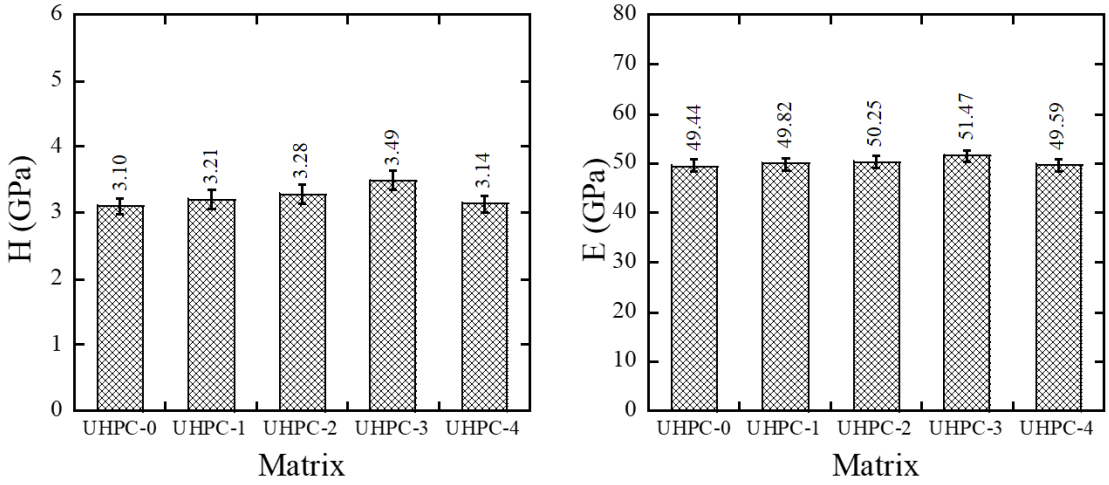

Figure 10. Hardness and Young's modulus of mixtures

Fig. 11 provides typical SEM images that reveal the influence of nano-$CaCO_3$ on the density of the ITZ within mixtures. It was observed that the UHPC-0 had porous areas, whereas UHPC-1, UHPC-2, UHPC-3, and UHPC-4 were homogeneous and dense. Scion Image analysis software was employed to evaluate the proportion of the porous area at ITZ based on the SEM images, as described in detail of studies [3, 25]. There are seven boundary layers originating from the fiber edge, with a uniform spacing of 10 μm between each layer of steel fibers embedded in mixtures. The porosity area ratio was calculated as the ratio of the porous area between two boundary layers to the total area encompassed by those layers. The percentage of porosity at ITZs surrounding fibers and mixtures corresponding to UHPC-0, UHPC-1, UHPC-2, UHPC-3 and UHPC-4 was 5.97 ± 0.96, 4.26 ± 0.72, 3.85 ± 0.55, 3.62 ± 0.24, and 4.66 ± 0.86%, respectively, as provided in Table 2. The incorporation of nano-$CaCO_3$ in UHPC led to lower porosity, attributed to its ability to improve particle packing and create a denser microstructure, which minimizes porous areas.

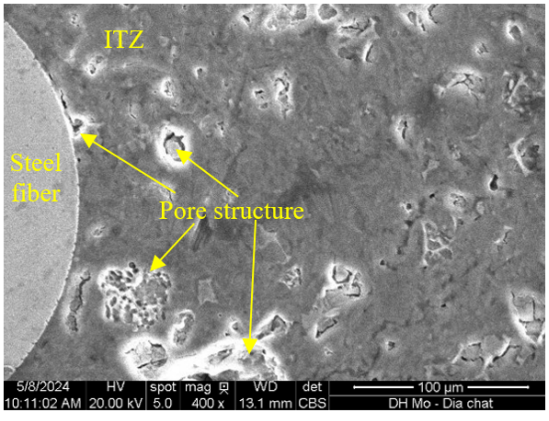

(a) UHPC-0

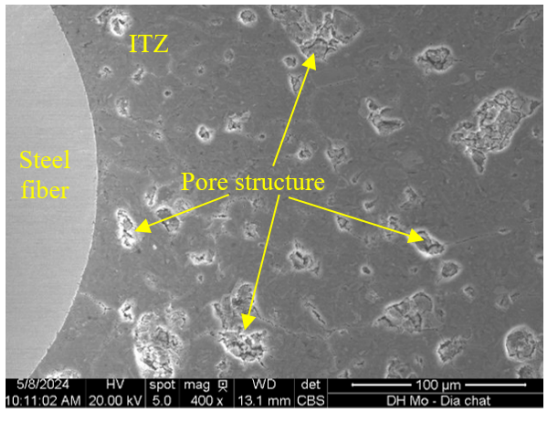

(b) UHPC-1

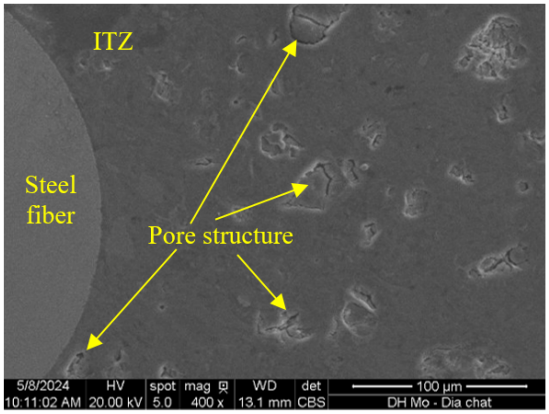

(c) UHPC-2

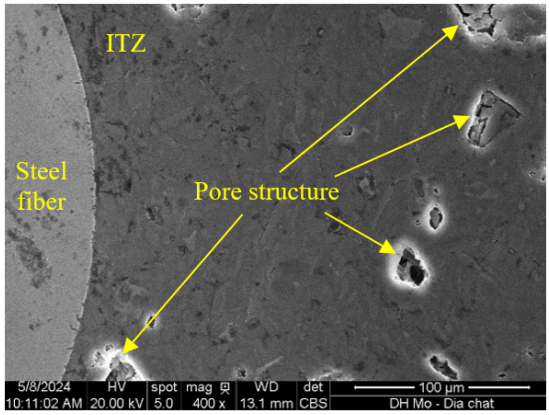

(d) UHPC-3

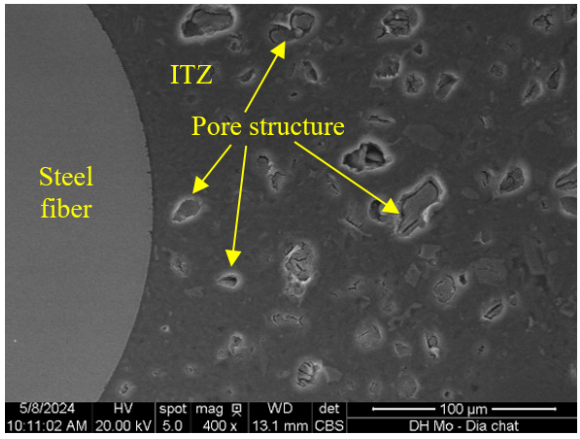

(e) UHPC-4

Figure 11. SEM images of the fiber–mixture interfaces of the mixtures

Table 2. The porous area at the ITZ of mixtures

Mixture	UHPC-0	UHPC-1	UHPC-2	UHPC-3	UHPC-4
Porosity (%)	5.97 ± 0.96	4.26 ± 0.72	3.85 ± 0.55	3.62 ± 0.24	4.66 ± 0.86

4. Conclusions

In this research, the effect of nano-$CaCO_3$ levels on the mechanical properties of the ITZ surrounding fiber and mixtures. The proportion of nano-$CaCO_3$ was adjusted to range from 1% to 4% based on the weight of the cement. Mini slump flow, compressive, and nanoindentation tests were conducted to evaluate the mechanical properties of UHPC. Besides, SEM was carried out to observe the surface characteristics and microstructures at the ITZ of mixtures. The conclusions derived from this study are as follows:

- The increase in nano-$CaCO_3$ content resulted in a reduction in the flowability of UHPC, with the slump flow decreasing from 185 ± 15 mm to 160 ± 5 mm as the content rose from 1% to 4%. This reduction is primarily due to the high surface area of the nano-$CaCO_3$, which absorbs more free water and superplasticizer, thereby raising the water demand of the mixtures.

- The incorporation of nano-$CaCO_3$ significantly enhanced the compressive strength of UHPC,

with improvements ranging from 1.47% to 9.49% as the content increased from 1% to 4%, due to better particle packing and a denser microstructure. However, as the nano-$CaCO_3$ content exceeded 3%, a slight reduction in strength was observed, likely caused by nanoparticle agglomeration and insufficient space for hydration products to develop fully.

- UHPC containing nano-$CaCO_3$ demonstrated higher both H and E at the ITZ in comparison to UHPC without any nano-$CaCO_3$. For instance, the H and E values of UHPC-3 were 3.49 ± 0.15 and 51.47 ± 1.23 GPa, respectively, while those for UHPC-0 were 3.10 ± 0.12 and 49.44 ± 1.22 GPa, respectively. This improvement in mechanical properties is attributed to the interfacial toughening effect induced by nanoparticles and the improved hydration of nano-$CaCO_3$. Additionally, SEM images indicated that UHPC with nano-$CaCO_3$ had denser and more uniform microstructures than UHPC without nano-$CaCO_3$.

References

[1] Shi, C., Wu, Z., Xiao, J., Wang, D., Huang, Z., Fang, Z. (2015). A review on ultra high performance concrete: Part I. Raw materials and mixture design. *Construction and Building Materials*, 101:741–751.

[2] Wang, D., Shi, C., Wu, Z., Xiao, J., Huang, Z., Fang, Z. (2015). A review on ultra high performance concrete: Part II. Hydration, microstructure and properties. *Construction and Building Materials*, 96: 368–377.

[3] Dang, V. P., Le, H. V., Kim, D. J. (2021). Loading rate effects on the properties of fiber-matrix zone surrounding steel fibers and cement based matrix. *Construction and Building Materials*, 283:122694.

[4] Xu, L., Deng, F., Chi, Y. (2017). Nano-mechanical behavior of the interfacial transition zone between steel-polypropylene fiber and cement paste. *Construction and Building Materials*, 145:619–638.

[5] Scrivener, K. L., Crumbie, A. K., Laugesen, P. (2004). The Interfacial Transition Zone (ITZ) Between Cement Paste and Aggregate in Concrete. *Interface Science*, 12(4):411–421.

[6] Elsharief, A., Cohen, M. D., Olek, J. (2003). Influence of aggregate size, water cement ratio and age on the microstructure of the interfacial transition zone. *Cement and Concrete Research*, 33(11):1837–1849.

[7] Yazıcı, H., Yardımcı, M. Y., Yiğiter, H., Aydın, S., Türkel, S. (2010). Mechanical properties of reactive powder concrete containing high volumes of ground granulated blast furnace slag. *Cement and Concrete Composites*, 32(8):639–648.

[8] Wu, Z., Shi, C., He, W. (2017). Comparative study on flexural properties of ultra-high performance concrete with supplementary cementitious materials under different curing regimes. *Construction and Building Materials*, 136:307–313.

[9] Wu, Z., Shi, C., Khayat, K. H. (2016). Influence of silica fume content on microstructure development and bond to steel fiber in ultra-high strength cement-based materials (UHSC). *Cement and Concrete Composites*, 71:97–109.

[10] Chan, Y.-W., Chu, S.-H. (2004). Effect of silica fume on steel fiber bond characteristics in reactive powder concrete. *Cement and Concrete Research*, 34(7):1167–1172.

[11] Zhang, W., Zeng, W., Zhang, Y., Yang, F., Wu, P., Xu, G., Gao, Y. (2020). Investigating the influence of multi-walled carbon nanotubes on the mechanical and damping properties of ultra-high performance concrete. *Science and Engineering of Composite Materials*, 27(1):433–444.

[12] Su, Y., Li, J., Wu, C., Wu, P., Li, Z.-X. (2016). Influences of nano-particles on dynamic strength of ultra-high performance concrete. *Composites Part B: Engineering*, 91:595–609.

[13] Yoo, D.-Y., Oh, T., Banthia, N. (2022). Nanomaterials in ultra-high-performance concrete (UHPC) – A review. *Cement and Concrete Composites*, 134:104730.

[14] Shaikh, F. U. A., Supit, S. W. M. (2014). Mechanical and durability properties of high volume fly ash (HVFA) concrete containing calcium carbonate (CaCO3) nanoparticles. *Construction and Building Materials*, 70:309–321.

[15] Xu, Q. L., Meng, T., Huang, M. Z. (2011). Effects of Nano-CaCO3 on the Compressive Strength and Microstructure of High Strength Concrete in Different Curing Temperature. *Applied Mechanics and Materials*, 121–126:126–131.

[16] Wu, Z., Khayat, K. H., Shi, C., Tutikian, B. F., Chen, Q. (2021). Mechanisms underlying the strength enhancement of UHPC modified with nano-SiO2 and nano-CaCO3. *Cement and Concrete Composites*, 119:103992.

[17] Sato, T., Diallo, F. (2010). Seeding Effect of Nano-CaCO3 on the Hydration of Tricalcium Silicate. *Transportation Research Record: Journal of the Transportation Research Board*, 2141(1):61–67.

[18] Lee, S. Y., Le, H. V., Kim, D. J. (2019). Self-stress sensing smart concrete containing fine steel slag aggregates and steel fibers under high compressive stress. *Construction and Building Materials*, 220: 149–160.

[19] Dang, V. P., Kim, D. J. (2023). Effects of nanoparticles on the tensile behavior of ultra-high-performance fiber-reinforced concrete at high strain rates. *Journal of Building Engineering*, 63:105513.

[20] ASTM C1437 (1993). *Standard test method for slump of hydraulic cement concrete*. ASTM International.

[21] ASTM C109/C109M-23 (2023). *Standard test method for compressive strength of hydraulic cement mortars*. ASTM International.

[22] Phi, D. V., Lam, T. V., Viet, L. H., Tuan, D. A., Thang, H. T., Tru, V. N. (2024). Effect of nano silica on interfacial bond strength of steel fiber embedded in ultra high performance concrete. *Journal of Materials and Construction*, 14(03):23–29. (in Vietnamese).

[23] Dang, V. P., Kim, D. J. (2023). Rate-sensitive pullout resistance of smooth-steel fibers embedded in ultra-high-performance concrete containing nanoparticles. *Cement and Concrete Composites*, 140:105109.

[24] Hoan, P. T., Thuong, N. T. (2021). Microstructural characteristics of ultra-high performance concrete by grid nanoindentation and statistical analysis. *Journal of Science and Technology in Civil Engineering (STCE) - NUCE*, 15(1):90–101.

[25] Thomson, J. G. (1919). Experiments on the Complement Fixation in Malaria with Antigens prepared from Cultures of Malarial Parasites (Plasmodium falciparum and Plasmodium vivax). *Proceedings of the Royal Society of Medicine*, 12(Med_Sect):39–48.

[26] Sridhar Babu, B., Kumaraswamy, A., Kumar, K. (2022). Effect of Macro, Micro and Nano Loads on The Indentation Behavior of Ti-6Al-4V and Haynes 242 Alloys. *International Journal of Automotive and Mechanical Engineering*, 19(2):9816–9822.

[27] Liu, X., Chen, L., Liu, A., Wang, X. (2012). Effect of Nano-CaCO3 on Properties of Cement Paste. *Energy Procedia*, 16:991–996.

[28] Wu, Z., Shi, C., Khayat, K. H., Wan, S. (2016). Effects of different nanomaterials on hardening and performance of ultra-high strength concrete (UHSC). *Cement and Concrete Composites*, 70:24–34.

[29] Wu, Z., Shi, C., Khayat, K. H. (2018). Multi-scale investigation of microstructure, fiber pullout behavior, and mechanical properties of ultra-high performance concrete with nano-CaCO3 particles. *Cement and Concrete Composites*, 86:255–265.

[30] Ghafari, E., Costa, H., Júlio, E., Portugal, A., Durães, L. (2014). The effect of nanosilica addition on flowability, strength and transport properties of ultra high performance concrete. *Materials & Design*, 59: 1–9.

[31] Rong, Z., Sun, W., Xiao, H., Jiang, G. (2015). Effects of nano-SiO2 particles on the mechanical and microstructural properties of ultra-high performance cementitious composites. *Cement and Concrete Composites*, 56:25–31.